JOURNAL OF THERMOPHYSICS AND HEAT TRANSFER
Vol. 10, No. 1, January–March 1996

Thermal Response of Radiantly Heated Spinning Spacecraft Booms

John D. Johnston* and Earl A. Thornton†
University of Virginia, Charlottesville, Virginia 22903

This article describes a study of the thermal response of radiantly heated spacecraft booms spinning about their principal axis. Thermally induced structural disturbances occur as the result of uneven solar heating and can reduce the pointing accuracy of a spin-stabilized spacecraft and in extreme cases affect the stability of the entire vehicle. The thermal response of radiantly heated spinning circular cross-sectional tubes is investigated using analytical, computational, and experimental approaches. An approximate analytical solution for the transient thermal response is presented. A finite element formulation is developed to evaluate the effects of natural convection, internal radiation, and temperature-dependent material properties on the thermal response. An experimental program undertaken to validate the analytical and computational models is described. The results of laboratory experiments conducted in the atmosphere are presented for a range of tube spin rates. Predictions from finite element analysis correlate well with experimental data and verify important aspects of spinning tube thermal behavior. Key aspects of the thermal behavior of radiantly heated spinning tubes are identified as 1) the independence of the tube average temperature of spin rate, 2) a decrease in the difference between maximum and minimum temperatures around the tube circumference with increasing spin rate, and 3) a shift in the steady-state temperature distribution in the direction of tube rotation.

Nomenclature

c = specific heat
h = tube wall thickness
h_{ir} = equivalent convection coefficient, internal radiation
h_{nc} = convection coefficient, natural convection
h_r = equivalent convection coefficient, external radiation
k = thermal conductivity
q = heat flux
R = tube radius
s = spatial coordinate
T = temperature
T_{av} = average temperature
T_p = perturbation temperature
T_{ss} = steady-state temperature
T_0 = initial temperature
T_∞ = exchange temperature
t = time
α = absorptivity
γ = thermal shift angle
ΔT = maximum temperature difference
δ = heat flux distribution parameter
ε = emissivity
ρ = density
σ = Stefan–Boltzmann constant
Φ = angular coordinate, Newtonian reference frame
ϕ = angular coordinate, rotating reference frame
ω = spin rate

Introduction

SPACECRAFT booms perform a variety of functions including use as antennae, supports for scientific payloads, structural members to support solar panels, and for gravity gradient stabilization. The space environment can affect boom performance adversely when interactions occur between these structures and solar radiation, magnetic fields, gravitational fields, and the atmosphere. One common interaction involves structural deformations induced through the action of uneven solar radiant heating. Thermally induced disturbances of spacecraft structures, particularly booms, can have a pronounced effect on the guidance, control, and pointing accuracy of space vehicles.

Thermally Induced Disturbances of Spacecraft Structures

During operations in space, structures are subjected to significant temperature gradients due to uneven solar radiant heating and cooling from thermal radiation to deep space. For example, the abrupt changes in the thermal loading of orbiting spacecraft that occur during orbital night/day transitions may lead to the development of significant temperature gradients in structures. Temperature gradients through the cross section of long, thin-walled booms cause thermal bending moments and torques to deform relatively flexible appendages. A survey of current literature by Thornton and Foster[1] reveals that thermally induced structural disturbances may be classified under three basic categories: 1) thermal snap, 2) thermally induced vibrations, and 3) thermal flutter. The effect of thermal snap is to impart a sudden impulsive moment or torque on a spacecraft due to rapid heating or cooling of an appendage. This phenomenon is illustrated by the disturbances experienced by the Upper Atmosphere Research Satellite (UARS) and the LANDSAT 4 and 5 satellites during orbital night/day transitions. Thermally induced vibrations are stable and may involve bending, torsional, or combined bending and torsional oscillations. These vibrations take place when the thermal response time of a boom is on the order of the period of the first vibration mode. The Hubble Space Telescope solar arrays provide a most noteworthy example of thermally induced vibrations. The most severe type of thermally induced disturbances is unstable oscillations that are termed thermal flutter. These oscillations are due to dynamic interaction between structural deformations and incident heating. Thermally induced dynamic motions of space-

Received April 24, 1995; presented as Paper 95-2019 at the AIAA 29th Thermophysics Conference, San Diego, CA, June 19–22, 1995; revision received Sept. 11, 1995; accepted for publication Sept. 14, 1995.

*Graduate Research Assistant, Department of Mechanical, Aerospace, and Nuclear Engineering. Student Member AIAA.
†Professor and Director, Light Thermal Structures Center. Associate Fellow AIAA.

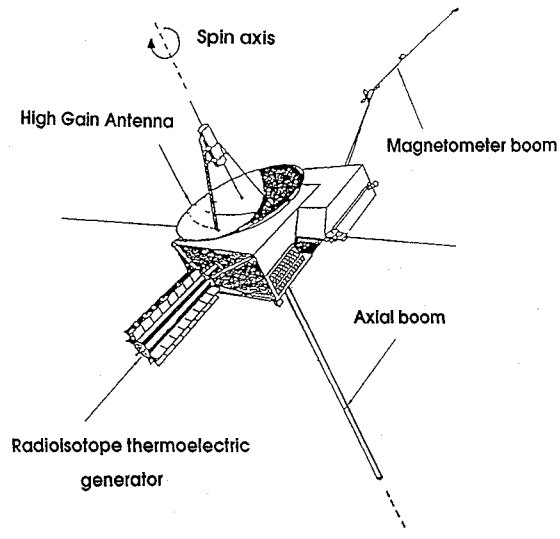

Fig. 1 Ulysses spacecraft.

craft booms can affect the stability of an entire spacecraft significantly. Since there are no external forces or moments associated with solar heating, the linear and angular momenta of the spacecraft are conserved, and the entire system responds dynamically about its c.m.

Booms attached to spin-stabilized spacecraft are subjected to periodic heating due to the spacecraft's rotation, which leads to more complicated behavior than that of nonspinning booms. The Canadian Aloutte I satellite was the first spin-stabilized spacecraft to experience performance degradation due to the effects of solar radiation on spacecraft appendages.[2] Following its launch in 1962, the satellite experienced spin decay due to boom deformation induced by the combined effects of solar heating and solar radiation pressure. The American spin-stabilized satellite Explorer XX experienced similar problems in 1964.[3] Thermally induced dynamic behavior of a spin stabilized spacecraft was again experienced on the Explorer-45 satellite in 1971.[4] This small scientific satellite was observed to have a nutation angle of approximately 7 deg. The problem was traced to thermal–elastic instability of the satellite's four booms. A unique example of thermally induced spacecraft motions and the motivation for this research is the anomalous behavior of the joint ESA/NASA solar exploration spacecraft Ulysses. The Ulysses, a spin-stabilized spacecraft whose mission is to explore the sun's polar regions, was launched from the Space Shuttle Discovery in 1990. The spacecraft began to experience anomalous nutational motions after an 8-m axial monopole antenna used to study radio and plasma waves was deployed approximately one month into the mission.[5] The cause of the wobble or nutation is attributed to thermally induced dynamic motions of the axial boom. The boom is a collapsible tube mast (CTM) made of beryllium copper and has a noncircular cross section. Figure 1 depicts the Ulysses spacecraft, showing the axial boom that is aligned with the spin axis of the spacecraft. The nutation induced by the axial boom motions is of amplitude significant enough to introduce a pointing error which, if uncompensated for by thruster firings, could result in a significant loss of scientific data from the mission.

Related Studies

A number of previous analytical and experimental studies have considered the problem of the thermal response of nonspinning and spinning spacecraft booms subject to radiant heating. Thornton and Kim[6] describe an analytical procedure for determining the unsteady temperature distribution in a nonspinning boom of circular cross section. Charnes and Raynor[7] investigated the steady-state temperature distribution on the surface of a spinning cylindrical space vehicle. The study used an approximate analytical solution to show that nonspinning cylinders exhibit greater temperature gradients than spinning cylinders, and that there is a shift in the location of the maximum and minimum temperatures on the surface of the cylinder due to its rotation. Mazur et al.[8] completed two experimental studies of the thermal response in gravity gradient rods in 1963. The first study investigated temperature gradients in 4.5-in.-long sections of coated and uncoated 0.50-in.-diam beryllium copper storable tubular extendible members (STEMs) using a collimated carbon arc-simulated solar source. The second study utilized large-scale thermal-vacuum facilities to test 20-ft-long sections of 0.5-in.-diam beryllium copper gravity gradient rods using an IR heat source. The studies showed that the use of silver plating to reduce surface absorbtivity is an effective means of reducing temperature gradients in spacecraft booms. Florio and Hobbs[9] studied steady-state temperature distributions of overlapped booms for the purpose of assessing thermal bending deformations in gravity gradient satellite booms and verified their analytical solutions with experimental results. Experiments were performed at the NASA Goddard Solar Simulation facility to determine temperature distributions of a number of representative test articles including a seamless stainless steel tube and a beryllium copper gravity gradient boom. The authors noted difficulties in establishing a constant heat flux intensity level and determining test article optical properties in their experimental study. Vigneron[10] investigated the thermal response time of thin-walled tubular booms subjected to constant and periodic heating. Thermal response time constants were developed analytically and verified experimentally for the case of satellite booms rotating end-over-end in the ecliptic plane. The problem of thermally induced vibrations of an axial boom on a spinning spacecraft has been treated analytically by Gulick.[11] The asymmetric cross section of the Ulysses axial boom was modeled as a circular cross section in the thermal analysis so that a tractable analytical solution could be obtained. The thermal analysis followed previous methods[6] developed for nonspinning booms and yielded steady-state results as well as an approach for determining the transient thermal response. Johnston[12] studied the thermal response of radiantly heated spinning cylindrical tubes and presents a detailed comparison of analytical, finite element, and experimental results for average temperatures, temperature gradients, and the positions of the steady-state maximum and minimum tube temperatures.

The thermal behavior of spinning axial booms differs significantly in several respects from that of nonspinning booms. The objective of this research is to develop a detailed understanding of the thermal behavior of radiantly heated spinning cylindrical spacecraft booms to provide information suitable for future experimental, computational, and analytical investigations of the thermally induced structural behavior of axial booms on spin-stabilized spacecraft. First, an approximate analytical solution for the transient thermal response is presented. Then, a finite element formulation is outlined that was implemented to provide comparison between computational and experimental results. Finally, an experimental program undertaken to investigate the thermal response of radiantly heated tubes under laboratory conditions is described. Experimental results are presented and comparisons are made between predictions from the approximate analytical solutions, finite element analysis, and experimental results.

Analytical Solutions

Analytical solutions for the thermal response of radiantly heated nonspinning and spinning circular cross-sectional spacecraft booms are approximate due to the nonlinear radiation heat transfer boundary condition and the nonuniform surface distribution of incident heat flux. Two approximate analytical solutions are considered: the first is a steady-state

solution that was obtained by Charnes and Raynor[7]; the second is a transient solution that was obtained following an approach outlined by Gulick.[11] An evaluation of these two approximate analytical solutions is presented by Johnston[12] for the case of an idealized circular cross-sectional axial boom on the Ulysses spacecraft. The evaluation was completed by comparing analytical predictions with results from finite element analysis. Details of the solution presented by Charnes and Raynor are given in Refs. 7 and 12. The following section outlines the approach for obtaining the approximate transient analytical solution.

Approximate Transient Analytical Solution

The analytical model assumes a radiantly heated thin-walled tube spinning about its principal axis. The geometry of the problem is depicted in Fig. 2. The tube is rotating at a constant rate ω in the counterclockwise direction. The incident heat flux q lies in a plane perpendicular to the spin axis of the tube. Two coordinate systems used in the solution of the problem are also shown in Fig. 2. The X-Y axes are located in a Newtonian reference frame fixed with respect to the rotation of the tube. The xx-yy axes are located in a rotating reference frame attached to the spinning tube. The principal axis of the tube coincides with both the Z axis and the zz axis perpendicular to the X-Y and xx-yy planes. The formulation of the problem is carried out in the rotating reference frame. The analytical model makes the following assumptions: 1) the cross section of the tube is circular; 2) the wall thickness of the tube is small in comparison to the tube radius ($h << R$) such that conduction through the thickness is negligible; 3) the tube length L is large compared to its radius R ($L >> R$); 4) conduction along the length of the tube is negligible; 5) the material properties of the tube are constant; 6) internal radiation is neglected; 7) radiant heating is via a constant, uniform heat flux in the X-Y plane; and 8) convective heat transfer is negligible. The problem is thus reduced to the case of one-dimensional transient conduction with a radiation boundary condition. The partial differential equation describing the system may be obtained from conservation of energy:

$$\frac{\partial T}{\partial t} - \frac{k}{\rho c R^2}\frac{\partial^2 T}{\partial \phi^2} + \frac{\sigma\varepsilon}{\rho c h}(T^4 - T_\infty^4) = \frac{\alpha\delta q}{\rho c h}\cos(\omega t + \phi) \quad (1)$$

where

$$\delta = 1: \quad (-\pi/2) \le (\phi + \omega t) \le (\pi/2)$$

$$\delta = 0: \quad (\pi/2) \le (\phi + \omega t) \le (3\pi/2)$$

The initial condition is

$$T(\phi, 0) = T_0 \quad (2)$$

The parameter δ given in Eq. (1) specifies that the boom is heated on one side only. The initial condition, given in Eq. (2) states the tube has a uniform initial temperature. An approximate solution to Eq. (1) was obtained following techniques outlined by Thornton and Kim[6] and Gulick.[11] There are three approximations made to solve the problem analytically. The temperature of the tube is approximated as the sum of an average temperature and a perturbation temperature:

$$T(\phi, t) = T_{av}(t) + T_p(\phi, t) \quad (3)$$

The average temperature $T_{av}(t)$ is a function only of time. The perturbation temperature $T_p(\phi, t) = T_m(t)\cos(\phi + \omega t - \gamma)$ is a function of both time and ϕ. The perturbation temperature in the rotating reference frame has a magnitude

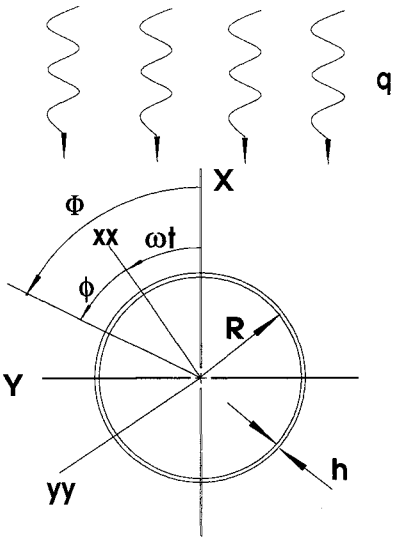

Fig. 2 Spacecraft boom analytical model and coordinate systems.

$T_m(t)$ and an orientation given by the cosine term that is a function of boom orientation $\phi + \omega t$ and γ. The rationale for this representation of the temperature is that the average temperature term corresponds to uniform heating, while the perturbation temperature term corresponds to the variation in heating due to the curved surface of the tube. The second approximation is that the perturbation temperature term is small in comparison to the average temperature term $T_p(\phi, t) << T_{av}(t)$. This allows the nonlinear radiation term in Eq. (1) to be expressed in the approximate form

$$T^4 \cong T_{av}^4 + 4T_{av}^4 T_p \quad (4)$$

In the final approximation, the discontinuous term $\delta\cos(\phi + \omega t)$ is expanded in a truncated Fourier series:

$$\delta\cos(\phi + \omega t) \cong (1/\pi) + \tfrac{1}{2}\cos(\phi + \omega t) \quad (5)$$

Substituting the three approximations in Eq. (1) gives the following two equations that are solved independently for the average and perturbation temperatures:

$$\frac{\partial T_{av}}{\partial t} + \frac{\sigma\varepsilon T_{av}^4}{\rho c h} = \frac{\sigma\varepsilon T_\infty^4}{\rho c h} + \frac{\alpha q}{\pi\rho c h} \quad (6a)$$

$$\frac{\partial T_p}{\partial t} - \frac{k}{\rho c R^2}\frac{\partial^2 T_p}{\partial \phi^2} - \frac{4\sigma\varepsilon T_{av}^3 T_p}{\rho c h} = \frac{\alpha q}{\rho c h}\frac{\cos(\phi + \omega t)}{2} \quad (6b)$$

The steady-state average temperature of the tube is obtained from Eq. (6a) as

$$T_{av,ss} = [T_\infty^4 + (\alpha q/\sigma\varepsilon\pi)]^{1/4} \quad (7)$$

and $T_{av}(t)$ is obtained by solving Eq. (6a) subject to the initial condition in Eq. (2). The result is

$$\frac{1}{T_{av,ss}^3}\left[\ln\frac{(T_{av,ss} - T_{av})(T_{av,ss} + T_0)}{(T_{av,ss} + T_{av})(T_{av,ss} - T_0)} + 2\tan^{-1}\frac{T_0}{T_{av,ss}} - 2\tan^{-1}\frac{T_{av}}{T_{av,ss}}\right] + \frac{\sigma\varepsilon}{\rho c h}t = 0 \quad (8)$$

The magnitude of the steady-state maximum perturbation temperature is obtained from Eq. (6b):

$$T_{mss} = \frac{\alpha q}{2\rho c h}\frac{\tau_{ss}}{\sqrt{1 + \omega^2\tau_{ss}^2}} \quad (9)$$

where τ_{ss} is defined as the steady-state thermal time constant for the tube:

$$\tau_{ss} = \left(\frac{k}{\rho c R^2} + \frac{4\sigma\varepsilon T_{av,ss}^3}{\rho c h}\right)^{-1} \tag{10}$$

Additionally, there exists a steady-state temperature shift angle γ_{ss} that determines the magnitude of the shift of the angular position of the maximum temperature in the direction of boom rotation:

$$\gamma_{ss} = \tan^{-1}(\omega\tau_{ss}) \tag{11}$$

The transient solution for the perturbation temperature is obtained using the method of complex variables as outlined by Gulick.[11] The final result is as follows:

$$T_p(\phi, t) = \left(\frac{\alpha q}{2\rho c h}\right)\frac{\tau_{ss}}{\sqrt{1 + \omega^2\tau_{ss}^2}}\left[\cos(\phi + \omega t - \gamma) - \exp\left(\frac{-t}{\tau_{ss}}\right)\cos(\phi - \gamma)\right] \tag{12}$$

The steady-state solution in the Newtonian (fixed) reference frame XY is the sum of two terms:

$$T_{ss}(\Phi) = T_{av,ss} + T_{mss}\cos(\Phi - \gamma_{ss}) \tag{13}$$

where $T_{ss}(\Phi)$ is the steady-state temperature, Φ is the angular coordinate in the fixed reference frame, and T_{mss} is the magnitude of the steady-state perturbation temperature. The difference between the maximum and minimum steady-state temperatures (or temperature gradient around the boom circumference) ΔT_{ss} is equal to two times the magnitude of the perturbation temperature

$$\Delta T_{ss} = T_{ss}(\Phi_{T\max}) - T_{ss}(\Phi_{T\min}) = 2T_{mss} \tag{14}$$

Remarks on Approximate Analytical Solution

Four observations about the thermal response of radiantly heated spinning tubes can be made from the solutions presented. First, from Eq. (7) the steady-state average temperature of a spinning tube is independent of spin rate and equal in magnitude to the steady-state temperature of a nonspinning tube. Second, from Eq. (9) the magnitude of the steady-state perturbation temperature is greatest for a nonspinning tube and decreases with increasing spin rate for spinning tubes. Third, from Eq. (12) as t approaches infinity, the perturbation temperature has a constant magnitude, but an orientation that varies with time in the rotating reference frame. Fourth, from Eq. (11) the shift in the position of the maximum and minimum steady-state temperatures increases to a predicted limiting value of 90 deg as tube spin rate approaches infinity.

Finite Element Analysis

A finite element analysis of the thermal response of radiantly heated spinning spacecraft booms was carried out to provide computational results for comparison with analytical predictions and experimental data. The solution obtained from the transient, nonlinear finite element analysis provides a good benchmark for evaluation of the approximate analytical solutions. Further, the finite element model allows the inclusion of the following effects not considered in the analytical solutions: material property variations with temperature, internal radiation, and external natural convection. The inclusion of these additional effects has particular value for simulation of the laboratory experiments.

The finite element model utilized in the computational study is the same physical model used in the transient analytical solution and is depicted in Fig. 2. The problem considers one-dimensional transient heat conduction around the circumference of a thin-walled cylindrical tube spinning about its principal axis at a constant rate ω subject to radiation and convection boundary conditions. The problem is governed by the following equation and initial condition:

$$c\rho h\frac{\partial T}{\partial t} - kh\frac{\partial^2 T}{\partial s^2} + h_r(T - T_\infty) + h_{nc}(T - T_\infty) + qrad_{int} - \alpha\delta q\cos(\phi_e + \omega t) = 0 \qquad T(s, 0) = T_0 \tag{15}$$

where $T = T(s, t)$ is the tube temperature, s is distance measured along the circumference of the tube ($s = \phi R$), ϕ_e is the element position angle, q is assumed constant over each element, h_{nc} is an external natural convection coefficient, h_r is an equivalent convection coefficient associated with external radiation, and $qrad_{int}$ is the internal radiation term. Convection coefficients are used to model heat transfer due to external convection as well as external and internal radiation. The equivalent convection coefficient for external radiation is developed following the methods outlined in Ref. 13. Since the external radiation heat transfer occurs due to exchanges between the tube surface and the surroundings, the nonlinear radiation boundary condition can be expressed through a temperature-dependent equivalent convection coefficient:

$$\sigma\varepsilon(T^4 - T_\infty^4) = h_r(T - T_\infty) \tag{16a}$$

where

$$h_r = \sigma\varepsilon(T^2 + T_\infty^2)(T + T_\infty) \tag{16b}$$

The nonlinear internal radiation term $qrad_{int}$ can also be expressed through an equivalent convection coefficient. Internal radiation exchanges are assumed to take place between the interior of the tube and an effective surroundings temperature equal to the average tube temperature. Thus,

$$qrad_{int} = h_{ir}(T - T_{av}) \tag{17a}$$

where

$$h_{ir} = \sigma\varepsilon_{int}(T^2 + T_{av}^2)(T + T_{av}) \tag{17b}$$

The external natural convection boundary condition has been modeled using an average natural convection coefficient. The natural convection coefficient is given in terms of a mean Nusselt number

$$h_{nc} = Nu_m k_f/L \tag{18}$$

where Nu_m is the mean Nusselt number, L is the characteristic length of the tube, and k_f is the thermal conductivity of air in the boundary layer. Expressions for the mean Nusselt number for a vertical cylinder are given by Kakac[14] and Holman.[15]

The computational approach[13] to the solution of the governing equation subject to the initial condition stated in Eqs. (15) involves nonlinear, transient analysis. The governing equations of the finite element formulation are derived using the method of weighted residuals. The finite element model of the cylindrical tube is discretized into N one-dimensional elements with r unknown nodal temperatures associated with each element. The approximate solution for the unknown nodal temperatures is given by

$$T(s, t) \approx \tilde{T}(s, t) = \sum_{i=1}^{r} N_i(s)T_i(t) = [N]\{T\} \tag{19}$$

This approximate solution is substituted into the governing equation over the domain of an individual element and the method of weighted residuals is applied using the Bubnov–Galerkin method. The Bubnov–Galerkin method uses the nodal interpolation functions for weighting functions. A two-node element ($r = 2$) was chosen for computations. The resulting element equations in matrix form are

$$[C]\left\{\frac{\partial T}{\partial t}\right\} + ([K_c] + [K_h])\{T\} = (\{R_q\} + \{R_h\}) \quad (20)$$

where $\{T\}$ are the unknown nodal temperatures, $[C]$ is the element capacitance matrix, $[K_c]$ is the element conductance matrix, $[K_h]$ is the element conductance matrix for convective terms, $\{R_q\}$ is the heat load vector due to the incident heat flux, and $\{R_h\}$ is the heat load vector due to convection. The formulation utilizes a consistent element capacitance matrix. Temperature-dependent material properties are constant over each element and are assumed to vary linearly with the element temperature. The numerical solution of the nonlinear transient equations requires time-marching and iterative solution techniques. The time-marching algorithm used is the Crank–Nicolson method. This implicit time-marching scheme is unconditionally stable and second-order accurate. The Newton–Raphson method is used to solve the nonlinear element equations iteratively at each time step. Full details of the finite element formulation are presented in Ref. 12. The finite element formulation was implemented in a special-purpose Fortran program for use in evaluating the approximate analytical solutions and for comparison with experimental results.

Experimental Study

The objective of the experimental study is to characterize 1) the transient behavior of the tube in terms of the average temperature as a function of time and 2) the long-time behavior in terms of steady-state average temperature, the steady-state temperature distribution, and steady-state thermal shift angles. Ground-based testing of model spacecraft booms provides important insight into the behavior of booms in space. However, space-simulated environmental conditions in the laboratory differ in several important ways from those of low Earth orbit and deep space. Radiative heating in the laboratory is provided typically by IR heat lamps utilizing quartz tube/tungsten filament heating elements. The heat flux produced by IR heat lamps differs from solar heating in that the space-simulated radiation has different spectral properties and is typically noncollimated. The hard vacuum of space is approximated by high vacuum chambers equipped with cooled shrouds that approximate the cold of deep space. The experiments described herein utilize an IR line heater and were conducted in the atmosphere.

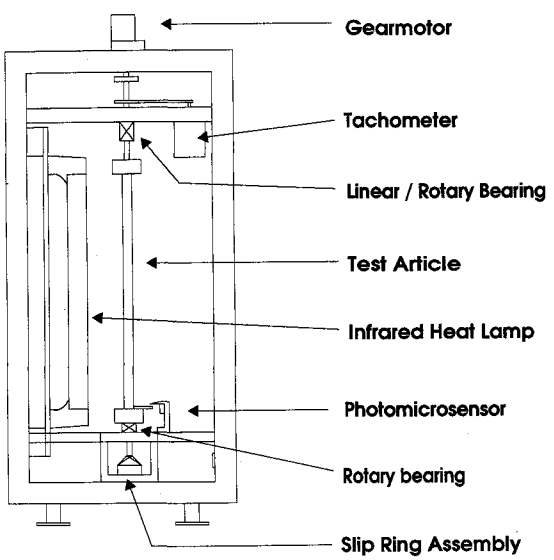

Fig. 3 Experimental test fixture.

Experimental Facility

A test fixture was designed and constructed for studying the thermal response of radiantly heated spinning tubes in the laboratory. The fixture consists of a 4 × 2 × 2 ft rectangular aluminum frame containing support structures for heating, test article, and instrumentation (Fig. 3). The test article is positioned parallel to the IR heater at a predetermined standoff distance. The tube is held at its ends by Rulon sleeves that act as insulators between the tube and the rotary drive mechanism. Rotary motion of the test article is provided by a permanent magnet d.c. gearmotor and an associated drive system. The drive system utilizes a series of timing belt pulleys for transferring the motion of the motor directly to the test article drive shaft. A timing belt/pulley arrangement was chosen to synchronize the driving and driven shafts and to provide smooth power transfer without the possibility of introducing slippage in the drive train. The system is capable of operating at constant spin rates ranging from 0.25 to 12.0 rpm. A tachometer coupled to the test article drive shaft using a timing belt/pulley arrangement measures the test article spin rate. A photomicrosensor provides information concerning the angular position of the test article. The photomicrosensor employs a light emitting diode (LED)/phototransistor arrangement that provides an output voltage that is altered by the presence of an obstruction or flag between the LED and the phototransistor. The photomicrosensor is placed in a shielded cage at a fixed position on the test frame and a flag is attached on the rotating test article. The flag is aligned such that the photomicrosensor signal is triggered when the position of the test article coincides with the primary thermocouple passing through the point $\Phi = 0$ deg (in the fixed reference frame coordinate system) on the test frame. Thus, the photomicrosensor is triggered each time the test article completes a revolution and passes through its initial position. This signal is used additionally to trigger the IR lamp controller initially such that the lamp turns on at the instant the test article is in the $\Phi = 0$-deg orientation.

Heating is provided by a quartz tube IR strip heater with a cooled parabolic reflector. The lamp utilizes a 2500-W clear quartz tube with a tungsten filament. Heating is directed perpendicular to the principal axis of the tube over a nominally 1.5-in.-wide by 26.0-in.-long strip. Incident heat flux levels were determined using an in-house lamp characterization test fixture. The lamp characterization procedure[16] provides a three-dimensional representation of the incident heat flux produced by the lamps, which was used as input to analytical and computational studies. The standoff distance of the test article was maintained at 3.75 in. for all tests. The IR heat lamp is controlled using a phase angle power controller that is regulated by a closed-loop control system for maintaining constant lamp power levels. The control system uses a line power transducer to provide feedback information to a personal computer-based control algorithm that controls a 4–20 mA current source that in turn regulates the power controller. The rise time required for the lamp to reach full power at a steady level is approximately 5 s.

Test Article

Figure 4 presents a schematic of a representative test article, instrumentation, and the test article drive mechanism. Test article temperatures are monitored using type T (copper-constantan) thermocouples with Teflon® insulation. Four 36-gauge thermocouples are spot welded at 90-deg increments around the exterior circumference of the test article. Signals from the thermocouples on the spinning test article are fed through a

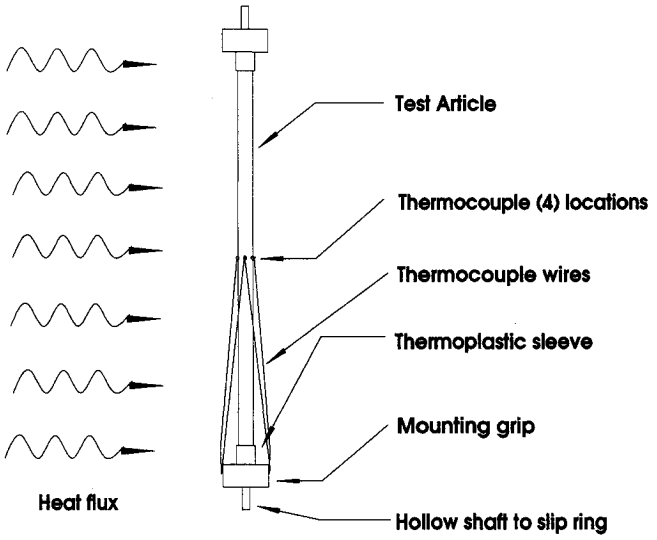

Fig. 4 Experimental test article.

slip-ring assembly for transmission to the stationary data acquisition system. All transducer signals are fed to a personal computer-based data acquisition system. Thermal tests were performed using thin-walled, closed-section stainless steel (304) tubes painted flat black with high-temperature paint to provide known surface optical properties. The tubes are 26.0 in. in length with a 1.0-in. o.d. and have a wall thickness of 0.020 in.

Test Procedure

The procedure followed in a typical test run begins with the test article at room temperature and the lamp cooling supply activated. The test article spin rate is adjusted to the desired value using the motor controller prior to the start of a test run. To begin a test, the drive motor is turned on and the test article is allowed sufficient time to attain a constant spin rate. The data acquisition system is then initiated and activates the IR lamp automatically when the test article returns to its initial orientation ($\Phi = 0$ deg) and triggers the photomicrosensor. Lamp line power is maintained at a constant level of approximately 720 W (corresponding to an average incident heat flux of 10,000 W/m^2) by the closed-loop control system for the duration of the test. The test continues for approximately 550 s. Since the test article average temperature reaches a steady-state value approximately 450 s after the lamp is turned on, this test duration allows for approximately 100 s of steady-state data. The test duration was lengthened for spin rates below 1.0 rpm so that steady-state data could be obtained over a complete revolution of the tube. The test article spin rate was varied between stationary and 12 rpm in the tests performed. For comparison, the Ulysses spacecraft is spin stabilized at a spin rate of 5 rpm.

Experimental Uncertainty

The estimated uncertainty in the temperature data is based on the limits of errors for the thermocouples and the data acquisition system. The limits of error for the type T thermocouples used in the experiments are given by the manufacturer as ± 1 K or $\pm 0.75\%$ of the full-scale reading, whichever is greater. For the experiments presented, the mean value for the steady-state average temperatures is 454 K, which would have an associated error of ± 3.4 K due to the thermocouples. The data acquisition system introduces uncertainty in the temperature data through three additional sources of error: system calibration, A/D computer board error, and the slip-ring mechanism. Calibration is completed using an independent calibration source specifically for use in setting the voltage offset level of a thermocouple channel on an A/D computer data acquisition board. The calibration is accurate to ± 0.6 K over the range calibrated (typically 250–700 K). The A/D computer board manufacturer specifies a typical error of $\pm 0.05\%$ of the full-scale reading, which corresponds to ± 0.2 K in the laboratory experiments. The final accuracy issue involves uncertainty imparted on the thermocouple signals by the slip-ring assembly. Although exact limits of error have not been established with respect to the slip ring, the errors are deemed insignificant for the following reasons. According to the manufacturer there are two potential sources of error: 1) errors due to the introduction of dissimilar metals and 2) errors due to differential heating at the ring/brush interface. Errors due to the introduction of dissimilar metals in the thermocouple circuit only occur when there is an end-to-end temperature gradient. Adequate care was taken to shield the slip ring from heating, which eliminates this as a source of error. According to the manufacturer, the slip ring utilized has insignificant ring/brush temperature differentials. Thus, the slip ring is neglected as a source of significant experimental uncertainty. An upper bound on the uncertainty in the temperature reading is given by the square root of the sum of the squares of the thermocouple, calibration, and computer board limits of error and was found to be ± 3.5 K.

Experimental Results

A series of tests was performed to determine the thermal response of a radiantly heated spinning tube under laboratory test conditions. Tube spin rate was held constant during each test run and varied between 0.0–12.0 rpm over the course of the test series. Table 1 summarizes the tests including representative values for the measured $T_{av,ss}$ and ΔT_{ss} from select test runs. These results show that the average temperature of the tube at steady state is independent of spin rate and has a mean value of 454 K for the test cases presented. Scatter in the data is attributed to slight variations in incident heat flux and the temperature of the surroundings between test runs. The results also demonstrate clearly the dependence of the maximum temperature difference on test article spin rate.

Figure 5 presents a plot of the average temperature history for the test article at a spin rate of 1.0 rpm. The tube reaches a maximum average temperature of 454 K in approximately 450 s. Test results show that the maximum temperature difference reaches a steady-state value in approximately 100 s for all spin rates. This demonstrates that the temperature

Table 1 Representative spinning tube temperatures

Spin rate, rpm	T_{av}, K	ΔT, K
0.0	455.2	109.1
0.25	452.5	92.4
0.50	452.6	68.9
0.75	455.6	53.1
1.0	453.7	41.1
1.5	452.8	30.2
2.0	453.4	22.3
2.5	455.3	18.2
3.0	452.3	15.7
3.5	453.9	13.3
4.0	450.2	12.2
4.5	454.5	10.8
5.0	451.2	9.3
5.5	452.3	8.6
6.0	452.9	8.0
7.0	455.2	7.4
8.0	453.8	6.3
9.0	455.8	6.0
10.0	454.2	5.5
12.0	453.4	4.9

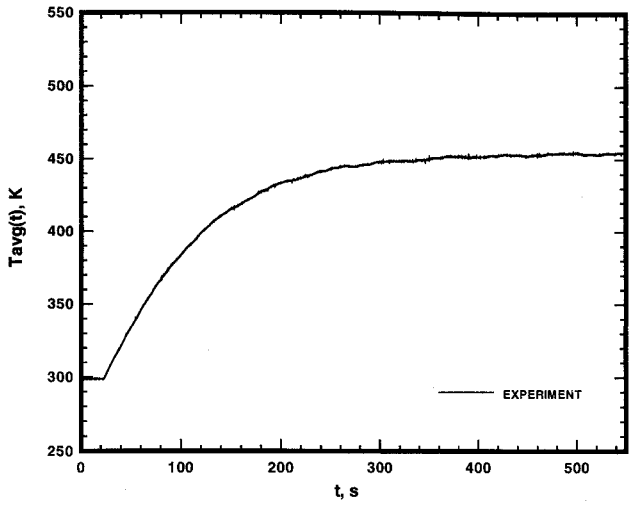

Fig. 5 Average temperature history for laboratory test article at 1 rpm.

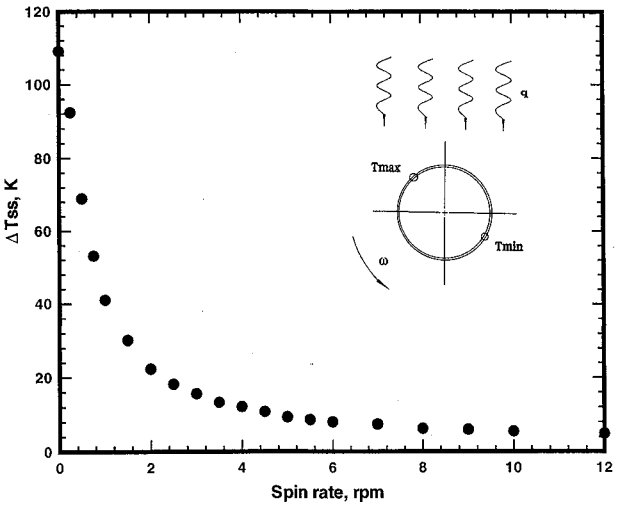

Fig. 7 Maximum temperature difference as a function of spin rate for laboratory test article.

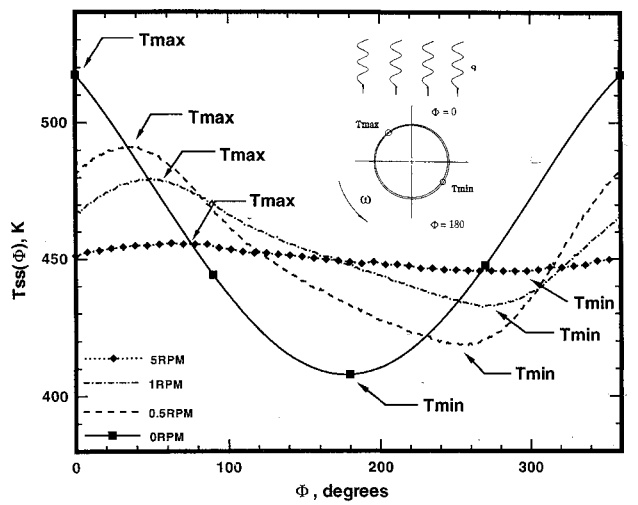

Fig. 6 Steady-state temperature distributions for laboratory test article.

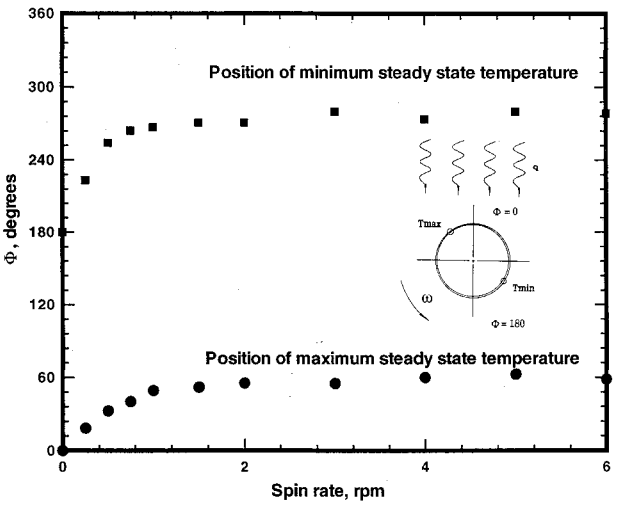

Fig. 8 Angular position of maximum and minimum temperatures as a function of spin rate for laboratory test article.

difference across a radiantly heated spinning tube develops at a much faster rate than the tube average temperature.

Steady-state temperature distributions around the circumference of the tube are presented in Fig. 6 for a representative range of spin rates. The curves in Fig. 6 are steady-state results obtained from four individual tests, each at a progressively greater constant spin rate. These results clearly show the decrease in the difference between the maximum and minimum tube temperatures as the spin rate increases progressively from 0.0 to 5.0 rpm. The locations of the maximum and minimum temperatures shift in the direction of tube rotation. The magnitude of these shifts is seen to grow larger as the spin rate increases.

Figure 7 presents values for the steady-state maximum temperature difference (temperature gradient) around the tube circumference for tests completed over a range of spin rates. The maximum temperature difference is greatest for a nonspinning tube and decreases for tubes with progressively greater spin rates. Figure 8 presents results showing the angular position of the steady-state maximum and minimum temperatures as a function of tube spin rate. The position of the maximum temperature shifts by a different amount than the position of the minimum temperature. The shift angles for both the maximum and minimum temperatures approach limiting values for spin rates above 2.0 rpm. The limiting value for the shift angle corresponding to the maximum temperature is approximately 60 deg, and the limiting value for the shift angle corresponding to the minimum temperature is approximately 280 deg. This shows that the angular separation of the maximum and minimum steady-state temperatures varies with spin rate. The angular separation is 180 deg for a nonspinning tube and increases to a limiting value of approximately 220 deg for tubes with progressively greater spin rates.

Comparison of Analysis and Experiment

Results from the experimental study are compared with numerical predictions obtained from the approximate analytical solution developed following the Gulick approach, the approximate analytical solution developed by Charnes and Raynor, and finite element analysis. The finite element model of the laboratory test article utilized 60 nodes, 60 equally spaced elements, and a time step of 0.25 s. Iteration at each time step proceeded until a convergence criterion was satisfied or after eight Newton–Raphson iterations had been completed. The convergence criterion requires that the normalized maximum nodal temperature change between iterations was less than 0.0001. The finite element model included the effects of temperature-dependent material properties, internal radiation, and external natural convection. Table 2 presents data for the test article used in the experimental study.

Figure 9 presents a series of curves based on experimental results, analytical predictions, and finite element analysis

Table 2 Test article data

Parameter	Value
R, m	0.0127
h, m	5.08E-4
k, W/m-K	15.0
c, J/kg-K	400.0
ρ, kg/m^3	8,000.0
α	0.825
ε	0.90
ε, internal	0.195
q, W/m^2	10,200
T_∞, K	290
T_0, K	290

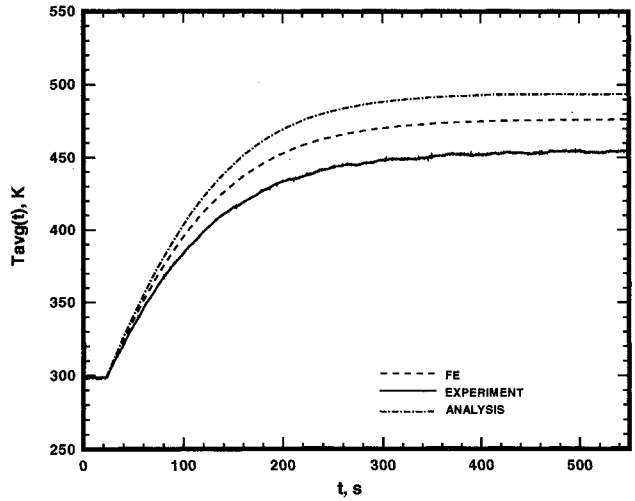

Fig. 9 Comparison of average temperature histories for laboratory test article at 1 rpm.

showing the average temperature history for the test article spinning at 1.0 rpm under laboratory test conditions. Results from the laboratory experiments show that the steady-state average temperature is 454 K. The approximate analytical solution [Eq. (8)], predicts a steady-state average temperature of 494 K. Thus, the prediction based on the analytical solution shows a difference of 40 K compared to the experimental result. The finite element analysis predicts a steady-state average temperature of 475 K, which has a difference of only 20 K compared to the experimental result. These results show that the approximate analytical solution given by Eq. (8) is not a good approximation for laboratory experiments conducted in the atmosphere when considering the average temperature response of a spinning tube. The presence of convection currents on the exterior surface of the tube leads to a decrease in tube temperatures from the values that would be obtained in a vacuum. The dominant component of the convective heat transfer is natural convection, based on the earlier result showing that steady-state average tube temperatures are independent of spin rate. If the average tube temperature decreased with increasing spin rate, then forced convection would be an important component of the overall heat transfer. Since the average temperatures are independent of spin rate, the dominant mode of convective heat transfer is natural convection.

Figure 10 presents a plot of steady-state maximum temperature difference for test article spin rates between 0.0–6.0 rpm. A comparison of experimental results, predictions from the approximate analytical solution Eq. (14), predictions from the Charnes and Raynor analytical solution, and finite element analysis all show good agreement for spin rates above 1.0 rpm. The decrease in the difference between the maximum and minimum steady-state temperatures with increasing spin

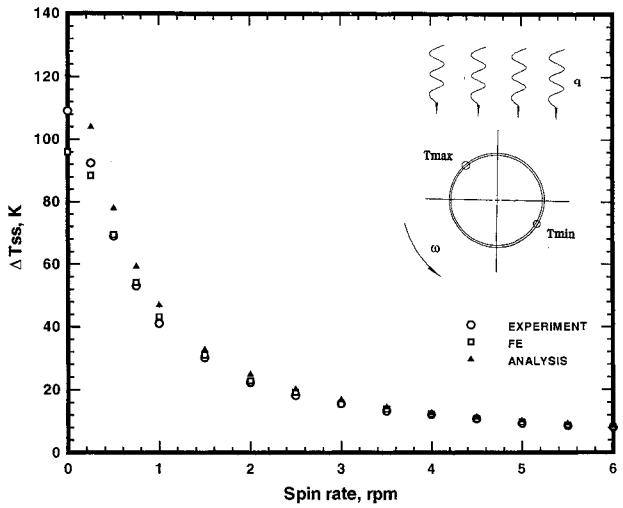

Fig. 10 Comparison of steady-state maximum temperature difference as a function of spin rate for laboratory test article.

rate is demonstrated by all three sets of results. The finite element predictions differ from the experimental results by 0.5–12%, predictions from the approximate analytical solution given in Eq. (14) differ from experimental results by 4.0–14.0%, and predictions from the Charnes and Raynor solution differ from experimental results by 2.0–6.0%. Both the approximate analytical solution developed by Charnes and Raynor and finite element analysis provide good results for laboratory experiments conducted in the atmosphere when considering the maximum temperature difference response of the tube. This is good news for the thermal-structural analyst, since the maximum temperature difference is an important parameter in thermally induced dynamics studies.

Comparing the steady-state experimental results presented in Table 1 with finite element predictions shows that including natural convection, internal radiation, and temperature-dependent material properties in the finite element model provides the best simulation of the laboratory experiments.[12] Additionally, the following observations can be made:

1) Modeling external natural convection improves the accuracy of the average temperature solution for the experiments conducted in the atmosphere.

2) Internal radiation effects are minor for the test article used in the experimental study.

3) Including temperature-dependent material properties improves the accuracy of the maximum temperature difference solution.

Conclusions

Analytical, computational, and experimental investigations of the thermal response of radiantly heated spinning cylindrical spacecraft booms were performed. An approximate analytical solution was presented for the transient thermal response of a spacecraft boom subject to radiant heating. A finite element formulation including the effects of natural convection, internal radiation, and temperature-dependent material properties was described. Laboratory experiments to characterize the thermal response of radiantly heated spinning tubes in the atmosphere were described, and results were presented for the average temperature histories and steady-state temperature distributions over a range of tube spin rates. Finally, predictions from the approximate analytical solutions and finite element analysis were compared with experimental results. Results show that finite element analysis including temperature-dependent material properties and natural convection provides the best correlation with experimental data for tests conducted in the atmosphere.

The thermal behavior of radiantly heated spinning tubes is characterized by a number of physical phenomena that were predicted by the analytical and finite element solutions and observed experimentally.

1) The response time of the temperature difference around the tube circumference is much shorter than the response time associated with the tube average temperature.

2) The magnitude of the steady-state average temperature is independent of tube spin rate.

3) The difference between maximum and minimum temperatures around the tube circumference (temperature gradient) is greatest for a nonspinning tube and decreases with increasing spin rate for spinning tubes.

4) The positions of the maximum and minimum tube temperatures shift in the direction of tube rotation.

5) The magnitude of the positional shifts associated with the maximum and minimum temperatures increases to different limiting values as the tube spin rate approaches infinity.

Acknowledgments

The research efforts of the authors were supported in part by the Light Thermal Structures Center through a Grant from the University of Virginia Academic Enhancement Program. We would like to recognize the efforts of Joe Blandino, Marshall Coyle, Rick Foster, and Rory McLeod of the Thermal Structures Laboratory for their contributions to this study.

References

[1]Thornton, E. A., and Foster, R. S., "Dynamic Response of Rapidly Heated Space Structures," *Computational Nonlinear Mechanics in Aerospace Engineering*, edited by S. N. Alturi, Vol. 146, Progress in Astronautics and Aeronautics, AIAA, Washington, DC, 1992, pp. 451–477.

[2]Etkin, B., and Hughes, P. C., "Explanation of the Anomalous Spin Behavior of Satellites with Long, Flexible Antennae," *Journal of Spacecraft and Rockets*, Vol. 4, No. 9, 1967, pp. 1139–1145.

[3]Hughes, P. C., and Cherchas, D. B., "Spin Decay of Explorer XX," *Journal of Spacecraft and Rockets*, Vol. 7, No. 1, 1970, pp. 92, 93.

[4]Flately, T. W., "Nutational Behavior of Explorer-45," *Significant Accomplishments in Science and Technology*, Goddard Space Flight Center, NASA SP-361, Jan. 1973, pp. 140–143.

[5]Peterson, H., "Ulysses, One Year After Launch," *4th European Symposium on Space Environmental Control Systems*, Vol. 2, ESA SP-324, Florence, Italy, 1991, pp. 951–955.

[6]Thornton, E. A., and Kim, Y. A., "Thermally-Induced Bending Vibrations of a Flexible Rolled-Up Solar Array," *Journal of Spacecraft and Rockets*, Vol. 30, No. 4, 1993, pp. 438–448.

[7]Charnes, A., and Raynor, S., "Solar Heating of a Rotating Cylindrical Space Vehicle," *ARS Journal*, Vol. 30, May 1960, pp. 479–484.

[8]Mazur, E. M., Matteo, D. N., and Oxenreider, R. S., "Passive Damper Bearing and Gravity-Gradient Rod Development," NASA SP-107, May 1965.

[9]Florio, F. A., and Hobbs, R. B., "An Analytical Representation of Temperature Distributions in Gravity Gradient Rods," *AIAA Journal*, Vol. 6, No. 1, 1968, pp. 99–102.

[10]Vigneron, F. R., "Thermal Curvature Time Constants of Thin-Walled Tubular Spacecraft Booms," *Journal of Spacecraft and Rockets*, Vol. 7, No. 10, 1970, pp. 1256–1259.

[11]Gulick, D. W., "Thermally-Induced Vibrations of an Axial Boom on a Spin-Stabilized Spacecraft," AIAA Paper 94-1556, April 1994.

[12]Johnston, J. D., "Thermal Response of Radiantly Heated Spinning Spacecraft Booms," M.S. Thesis, Dept. of Mechanical, Aerospace, and Nuclear Engineering, Univ. of Virginia, Charlottesville, VA, Aug. 1995.

[13]Huebner, K. H., Thornton, E. A., and Byrom, T., *The Finite Element Method for Engineers*, 3rd ed., Wiley, New York, 1995.

[14]Kakac, S., Shah, R. K., and Aung, W., *Handbook of Single-Phase Convective Heat Transfer*, Wiley, New York, 1987.

[15]Holman, J. P., *Heat Transfer*, 7th ed., McGraw–Hill, New York, 1990.

[16]Thornton, E. A., Coyle, M. C., and McLeod, R. N., "Experimental Study of Plate Buckling Induced by Spatial Temperature Gradients," *Journal of Thermal Stresses*, Vol. 17, 1994, pp. 191–212.